J|A|C|S ARTICLES

Published on Web 11/30/2010

Binding Energies and Isomerization in Metallocene Ions from Threshold Photoelectron Photoion Coincidence Spectroscopy

Ágnes Révész,[†,II] László Szepes,[†] Tomas Baer,[‡] and Bálint Sztáray*[,§]

Institute of Chemistry, Eötvös Loránd University, Budapest, Hungary, Department of Chemistry, University of North Carolina, Chapel Hill, North Carolina 27599, United States, and Department of Chemistry, University of the Pacific, Stockton, California 95211, United States

Received June 23, 2010; E-mail: bsztaray@pacific.edu

Abstract: Metallocene ions (Cp_2M^+, M = Cr, Co, Ni) were studied by threshold photoelectron photoion coincidence spectroscopy (TPEPICO) to investigate the mechanism, energetics, and kinetics of the ionic dissociation processes. The examined energy-selected Cp_2M^+ ions fragment by losing the neutral cyclopentadienyl ligand. In addition, CH and C_2H_2 losses appear as minor channels, while the cobaltocene ion also loses an H atom. A possible isomerization pathway has also been observed for Cp_2Ni^+, yielding a complex with pentafulvalene ($C_{10}H_8$) with a loss of H_2. In order to determine the 0 K appearance energies for the CpM^+ fragment ions, the asymmetric time-of-flight peak shapes and the breakdown diagrams of the energy-selected metallocene ions were modeled by both the rigid activated complex (RAC) Rice−Ramsperger−Kassel−Marcus (RRKM) theory and the simplified statistical adiabatic channel model (SSACM). The following appearance energies were obtained with SSACM, which is more reliable for loose transition states: 10.57 ± 0.14, 11.01 ± 0.13, and 10.18 ± 0.13 eV for M = Cr, Co, and Ni, respectively. These values combined with the corresponding adiabatic ionization energies yield M−Cp bond dissociation energies in Cp_2M^+ ions of 5.04 ± 0.16, 5.77 ± 0.15, and 3.96 ± 0.15 eV. Density functional calculations at the B3LYP/6-311G(d,p) level of theory were used to determine the structures of these complexes and to provide parameters necessary for the analysis of the experimental data. The trends in the M−Cp bond energies can be related to the electronic structures of the metallocene ions based on a simple molecular orbital picture.

Introduction

Metallocenes and their derivatives represent a particularly important and interesting class of organometallic complexes as they are widely used as catalysts[1−7] and chemical vapor deposition (CVD) precursors.[8−12] Therefore, the dissociation kinetics and energetics, especially the metal−ligand bond energies, are of great importance. However, their thermochemistry is not well-known and the ionic bond energies found in the literature show considerable uncertainties, partly because the thermal energy distributions and the kinetic shift are generally neglected in the data analyses. In the past few years, our groups have investigated the gas-phase ionic dissociation of a number of organometallic complexes, such as $CpMn(CO)_3$,[13] $CpCo(CO)_2$,[14,15] $C_6H_6Cr(CO)_3$,[16] Cp_2Mn,[17] $(C_6H_6)_2Cr$,[18] and $Co(CO)_3NO$[19] (where Cp = C_5H_5, cyclopentadienyl ligand) and their substituted analogues[20−22] using threshold photoelectron photoion coincidence spectroscopy (TPEPICO). It was demonstrated that this technique is a useful tool to obtain accurate metal−ligand bond dissociation energies. In the present study, we have investigated the mechanism, energetics, and kinetics of the ionic dissociation processes of chromocene, cobaltocene, and nickelocene and determined the $[CpM−Cp]^+$ bond dissociation energies.

[†] Eötvös Loránd University.
[‡] University of North Carolina, Chapel Hill.
[§] University of the Pacific.
[II] Current address: Institute of Organic Chemistry and Biochemistry, Flemingovonám. 2, 16610 Prague 6, Czech Republic.

(1) Resconi, L.; Cavallo, L.; Fait, A.; Piemontesi, F. *Chem. Rev.* **2000**, *100*, 1253.
(2) Hlatky, G. G. *Chem. Rev.* **2000**, *100*, 1347.
(3) Lenges, C. P.; Brookhart, M.; Grant, B. E. *J. Organomet. Chem.* **1997**, *528*, 199.
(4) Luo, X. X.; Zhao, X.; Xu, S. S.; Wang, B. Q. *Polymer* **2009**, *50*, 796.
(5) Blom, R.; Dahl, I. M.; Swang, O. *J. Catal.* **2000**, *194*, 352.
(6) Hoshino, M.; Ebisawa, F. *J. Appl. Polym. Sci.* **1998**, *70*, 441.
(7) Elschenbroich, C. *Organometallics*, 3rd ed.; Wiley−VCH Verlag: Weinheim, Germany, 2006; pp 484−528.
(8) Dowben, P. A.; Kizilkaya, O.; Liu, J.; Montag, B.; Nelson, K.; Sabirianov, I.; Brand, J. I. *Mater. Lett.* **2009**, *63*, 72.
(9) Brissoneau, L.; Sahnoun, R.; Mijoule, C.; Vahlas, C. *J. Electrochem. Soc.* **2000**, *147*, 1443.
(10) Xiang, R.; Luo, G. H.; Yang, Z.; Zhang, Q.; Qjan, W. Z.; Wei, F. *Mater. Lett.* **2009**, *63*, 84.
(11) Kunadian, I.; Andrews, R.; Menguc, M. P.; Qian, D. *Chem. Eng. Sci.* **2009**, *64*, 1503.
(12) Yadav, R. M.; Dobal, P. S.; Shripathi, T.; Katiyar, R. S.; Srivastava, O. N. *Nanoscale Res. Lett.* **2009**, *4*, 197.
(13) Li, Y.; Sztáray, B.; Baer, T. *J. Am. Chem. Soc.* **2001**, *123*, 9388.
(14) Sztáray, B.; Baer, T. *J. Am. Chem. Soc.* **2000**, *122*, 9219.
(15) Sztáray, B.; Szepes, L.; Baer, T. *J. Phys. Chem. A* **2003**, *107*, 9486.
(16) Li, Y.; McGrady, J. E.; Baer, T. *J. Am. Chem. Soc.* **2002**, *124*, 4487.
(17) Li, Y.; Sztáray, B.; Baer, T. *J. Am. Chem. Soc.* **2002**, *124*, 5843.
(18) Li, Y.; Baer, T. *J. Phys. Chem. A* **2002**, *106*, 9820.
(19) Sztáray, B.; Baer, T. *J. Phys. Chem. A* **2002**, *106*, 8046.
(20) Gengeliczki, Zs.; Sztáray, B.; Baer, T.; Iceman, C.; Armentrout, P. B. *J. Am. Chem. Soc.* **2005**, *127*, 9393.
(21) Révész, Á.; Pongor, Cs. I.; Bodi, A.; Sztáray, B.; Baer, T. *Organometallics* **2006**, *25*, 6061.
(22) Gengeliczki, Zs.; Szepes, L.; Sztáray, B.; Baer, T. *J. Phys. Chem. A* **2007**, *111*, 7542.

So far, only one paper has been published on the electron ionization (EI) mass spectrometry of chromocene, by Müller and D'Or.[23] In that study, the authors determined the $[CpCr-Cp]^+$ bond dissociation energy as the difference of the appearance energies (AE) measured for Cp_2Cr^+ and $CpCr^+$ using the method suggested by Warren,[24] arriving at a value of 6.55 ± 0.15 eV. In the same work, $[CpM-Cp]^+$ bond energies of 7.79 ± 0.15 and 5.43 ± 0.15 eV were obtained for M = Co and Ni, respectively. In addition, several other metallocene ion fragmentation channels have been observed, but their intensity was too low for quantitative analysis. There are three other early works on the electron ionization mass spectrometry of cobaltocene, which reported $CpCo^+$ AEs of 12.3 ± 1 eV,[25] 13.2 ± 0.2 eV,[26] and 14.0 ± 0.3 eV.[27] However, as indicated previously, these values have significant errors because of the low energy resolution of EI experiments, unfavorable threshold laws, and most importantly, the neglect of kinetic shift. In a more recent electron ionization study,[28] considerable efforts were made to take the kinetic shift into account. The dissociation onsets were measured by monitoring the fragment ions generated from metastable parent ions, and the thresholds were calculated by extrapolation of the log(ion intensity) versus electron energy to a vanishing ion intensity, which gave a $CpCo^+$ appearance energy of 10.21 ± 0.30 eV and a $[CpCo-Cp]^+$ dissociation energy of 4.86 ± 0.50 eV. For $CpNi^+$ appearance energies, several data can be found in the literature, again from electron ionization mass spectrometric investigations. Pignataro and Lossing[25] reported a value of 11.9 ± 1.0 eV, while values of 12.4 ± 0.3 and 12.6 ± 0.2 eV were published by Schissel et al.[29] and Begun and Compton,[27] respectively. The highest number (13.0 ± 0.25 eV) comes from Flesch et al.,[30] which leads to a predicted ionic bond energy larger than 6 eV. Other groups have performed time-resolved photodissociation rate measurements on the nickelocene cation at two different UV wavelengths in an ion cyclotron mass spectrometer.[31] Rice–Ramsperger–Kassel–Marcus (RRKM) theory was used to extrapolate the two rate constants to zero internal energy, and the reported bond energy was 3.24 ± 0.07 eV.

In the present work, energy-selected Cp_2M^+ (M = Cr, Co, Ni) ions have been prepared and their gas-phase unimolecular dissociation kinetics have been studied with the TPEPICO technique. The experimental results along with the statistical analysis of the dissociation rates and energetics provide accurate E_0 values of the fragment ions, from which accurate bond energies of the ionic species could be obtained. The determined bond dissociation energies are discussed in terms of the electronic structure of the Cp_2M^+ ions.

Experimental Approach

All experimental data presented here were obtained by the TPEPICO experiment that has been described in detail previously.[32,33] The sample was leaked into the ionization region of the TPEPICO spectrometer through a temperature-controlled direct sample inlet system. It was necessary to heat the solid sample to 60 °C (Cp_2Cr), 70 °C (Cp_2Co), or 55 °C (Cp_2Ni) to obtain sufficient vapor pressure. The sample molecules were ionized with vacuum ultraviolet (VUV) light emitted from a H_2 discharge lamp, dispersed by a 1-m normal incidence monochromator with a resolution of 1 Å (8 meV at 10 eV photon energy). The VUV wavelengths were calibrated against the hydrogen Lyman-α resonance line. The ions and the electrons were extracted in opposite directions with an electric field of 20 V/cm. The electrons traveled 6.8 mm through this region before they were accelerated by use of velocity focusing optics[32] into a 13 cm long drift region maintained at about 70 eV. With this lens, electrons with zero velocity perpendicular to the extraction field are focused to a point at the end of the flight tube, whereas electrons with nonzero perpendicular velocity are focused onto rings around this central spot with radii according to their initial perpendicular velocity component. A mask placed at the end of the electron drift tube contained a central 1.4 mm hole and a 2 × 8 mm rectangular opening for the hot electrons. The electrons passing through these two apertures were detected by two Channeltron electron detectors. Assuming that the signal in the off-axis detector was proportional to the energetic (hot) electron contribution in the central spot, a weighted fraction of the outer "ring" signal is subtracted from the central electrode signal, thereby correcting the threshold electron signal for the contribution of initially energetic electrons.[33]

In the linear time-of-flight ion optics setup, the ions were accelerated in the same 20 V/cm field over approximately 5 cm to 104 eV. A short second acceleration region, terminated by grids, increased the ion energy to 260 eV. The ions proceeded to a 26-cm-long field-free drift region and were subsequently decelerated with a −100 V voltage difference. This deceleration slowed down the fragment ions produced in the drift region more than parent ions and thus allowed the separation of these fragment ions from their precursor ions. After drifting through the 8-cm-long second field-free region, the ions were detected with a Chevron stack of multichannel plates. Nickelocene was also measured with a reflectron time-of-flight setup (ReTOF) in order to investigate the H_2 loss from the parent ion. The reflectron gives far superior mass resolution; therefore, the parent ion peak and the peak of H_2 loss are well-separated. However, slowly dissociating ions might be lost in the reflectron, if the mass difference between the parent and daughter ion is large, so this setup is not ideally suited for investigating the cyclopentadienyl loss from metallocene ions. After exiting the 5-cm-long first acceleration region, the ions entered the 38-cm-long drift region of the ReTOF, which ended in a 24-cm-long soft reflectron where the ions were reflected by a voltage of 141 V. After traversing the second 35-cm-long drift region, they were detected with a Chevron stack of multichannel plates. In both setups, the electron and ion signal served as start and stop signal for the acquisition of the ion time-of-flight (TOF) spectra, and the TOF for each delayed coincidence event was stored in an Ortec multichannel analyzer. Because both the center and the ring electron signals served as start signals, two TOF distributions were obtained at each photon energy. TOF distributions were collected for 1–24 h depending on the signal intensity and the desired spectrum quality. The weighted fraction of the TOF distribution generated by the ring electrode signal was subtracted from the center electrode signal to correct for the hot electron contribution.

The TPEPICO spectra were used for two purposes. First, the fractional abundances of the parent and daughter ions were calculated as a function of the photon energy (breakdown diagram). Second, ion decay rates were extracted from asymmetric TOF distributions of the daughter ion signal. This asymmetry is the result of slowly dissociating (metastable) ions dissociating in the 5-cm acceleration region, resulting in a time-of-flight between the parent and the daughter ion's flight time. In addition to this asymmetry, a Gaussian-shaped peak (the drift peak) appears at a TOF larger than the parent ion's flight time, which is due to metastable ions dissociating in the first field-free drift region. The ions that dissociate

(23) Müller, J.; D'Or, L. *J. Organomet. Chem.* **1967**, *10*, 313.
(24) Warren, J. W. *Nature* **1950**, *165*, 810.
(25) Pignataro, S.; Lossing, F. P. *J. Organomet. Chem.* **1967**, *10*, 531.
(26) Puttemans, J. P.; Hanson, A. *Ing. Chim.* **1971**, *53*, 17.
(27) Begun, G. M.; Compton, R. N. *J. Chem. Phys.* **1973**, *58*, 2271.
(28) Opitz, J. *Int. J. Mass Spectrom.* **2003**, *225*, 115.
(29) Schissel, P.; McAdoo, D. J.; Hedaya, E.; McNeil, D. W. *J. Chem. Phys.* **1968**, *49*, 5061.
(30) Flesch, G. D.; Junk, G. A.; Svec, H. J. *J. Chem. Soc., Dalton Trans.* **1972**, 1102.
(31) Lin, C.-Y.; Dunbar, R. C. *J. Phys. Chem.* **1995**, *99*, 1754.
(32) Baer, T.; Li, Y. *Int. J. Mass Spectrom.* **2002**, *219*, 381.
(33) Sztáray, B.; Baer, T. *Rev. Sci. Instrum.* **2003**, *74*, 3763.

after the last acceleration region are detected as parent ions. Similarly, in the ReTOF setup, slowly dissociating ions dissociating in the first acceleration region result in a quasi-exponential shaped daughter ion peak. This asymmetric daughter ion peak is terminated by a Gaussian-shaped peak that is due to ions that dissociate between the acceleration region and the entry into the reflectron. The fractional abundances and the direct kinetic information were used together in the data analysis as described later.

The chromocene, cobaltocene and nickelocene samples were purchased from Strem Chemicals and were used without further purification.

Quantum Chemical Calculations. The modeling of the experimental data requires vibrational frequencies and rotational constants of the relevant neutral and ionic species. These were determined from quantum chemical calculations, which were performed with the Gaussian 03 package.[34] All the calculations were carried out by use of density functional theory (DFT), with the B3LYP[35] exchange−correlation functional and the 6-311G(d,p) basis set.[36]

The data were analyzed by both the rigid activated complex (RAC) RRKM theory and the simplified statistical adiabatic channel model (SSACM). Both models require vibrational frequencies of the dissociating ions. RRKM also requires approximate transition-state frequencies, while SSACM requires only the vibrational frequencies of the products. For the calculation of the internal energy distribution of the neutral Cp_2M, one also needs to calculate the vibrational frequencies of the neutral molecules. Geometries of the relevant species were therefore optimized at the above DFT level; the minima were confirmed by the absence of imaginary frequencies. Various spin states were considered for the neutral molecules and parent ions, and the lowest-lying states were chosen to determine the vibrational frequencies[13] used in the modeling. The spin state of the neutral molecules was determined to be the triplet for chromocene, doublet for cobaltocene, and triplet for nickelocene, while the lowest energy spin multiplicities ($2S + 1$) in the ions are 4, 1, and 2 for the Cp_2M^+ ions with M = Cr, Co, and Ni, respectively. The lowest-energy spin multiplicities for the Cp-loss dissociation products were calculated to be 5, 4, and 3 for CpM^+ with M = Cr, Co, and Ni, respectively. The doublet state of $CpCo^+$ is very close in energy to the quartet, but the bond energy trend (vide infra) is more consistent with assumption of a quartet state. Although the dissociation of singlet Cp_2Co^+ to quartet $CpCo^+$ is formally spin-forbidden, TPEPICO studies on a similar $CpMn(CO)_3^+$ ion clearly showed that spin conservation laws can be violated in such dissociations.[13] Structure and frequencies were also computed for the $(C_{10}H_8)NiH_2^+$ species (where $C_{10}H_8$ = pentafulvalene), formed via isomerization of Cp_2Ni^+ (see later).

The Cp loss reactions of the Cp_2M^+ ions are expected to be direct dissociation reactions without reverse activation barrier.[17] In addition, we handled the other channels as direct dissociations as well, which gave a good fit for cobaltocene and nickelocene and resulted in an adequate description of the minor dissociation channel of chromocene. Because the dissociations are expected to proceed without a reverse barrier, the transition states do not correspond to a critical point on the potential energy surface. To approximate the structure and vibrational frequencies of the transition states for the RAC-RRKM calculations, the metal−cyclopentadienyl bond distance of the leaving cyclopentadienyl groups was fixed at 5.0 Å, and the geometry was optimized with respect to the remaining coordinates. In the case of the minor dissociation channels, namely, H, CH, C_2H_2, and H_2 loss, the precursor ions' frequencies were used as estimates for the frequencies of the transition states, and one frequency, which was assigned as the critical frequency for the dissociation step, was deleted. Since, in the RAC-RRKM model, the transition-state (TS) frequencies were used only as a starting point in the fitting to the experimental dissociation rate curves, the accuracy of the TS frequencies was not a concern, and therefore no frequency scaling factors were used in any of the quantum-chemical calculations. The lowest few frequencies of the transition states, which turn into product rotations and translations, were adjusted to fit the calculated TOF distributions and breakdown diagrams to the experimental ones.

In the SSACM analysis, one needs the vibrational frequencies of the product ions and neutral fragments instead of those of the rigid transition states. Thus, calculations were carried out for the Cp, C_2H_2, CH, and H_2 neutrals and the $C_8H_8Cr^+$, $C_{10}H_9Co^+$, $C_9H_9Co^+$, $C_8H_8Co^+$, $C_9H_9Ni^+$, $C_8H_8Ni^+$, $C_{10}H_8Ni^+$, and CpM^+ (M = Cr, Co, Ni) ions. According to the lowest energy geometries in our calculations, the $C_9H_9M^+$ species contain a cyclopentadienyl and a cyclobutadienyl ligand, whereas in $C_8H_8M^+$ there is a cyclopentadienyl and an allyl group bound to the metal center (M = Co, Ni). While a C_2H_2 loss leading to an allyl group seems quite reasonable, it is hard to find a qualitative explanation for the CH loss channel, even if cyclo-C_4H_4 is quite stable complexed to a transition metal center. In the case of $C_8H_8Cr^+$, there are two other species besides the above-mentioned structure that are very close in energy: the first one has a cyclooctatetraene ligand, while the other one contains a dihydropentalene group. Since there is not enough experimental information to distinguish the three alternative dissociation pathways, the C_2H_2 loss was treated analogously to the Co- and Ni-containing species in the data analysis. However, the existence of the other dissociation channels cannot be excluded and may warrant a variable-energy cross-beam experiment, such as the one described by Dutuit and co-workers,[37] to search for isomer-specific association reactions. Again, the geometry optimizations were carried out with several spin states, and the equilibrium structures of the lowest-energy species were confirmed by the absence of negative frequencies.

In order to compare the experimentally derived binding energies, the 0 K M−Cp bond energies were estimated computationally by carrying out counterpoise (CP) corrected[38] single-point B3LYP/6-311++G(2df,2pd)[36a,39] calculations on the above geometries. Zero-point vibrational energies (ZPVE) were also taken from the B3LYP/6-311G(d,p) calculations. The computed vibrational frequencies were not scaled with the usual scaling factors determined for a set of organic molecules, because even if these frequency scaling factors were reliable for the organometallic species, the error introduced into the ΔZPVE is less than a few millielectronvolts. It is worth mentioning that the magnitude of the counterpoise correction in the single-point calculations with the large, 6-311++G(2df,2pd) basis set is on the order of 0.05 eV. Test calculations moreover showed that the effect of applying the CP correction to the optimization with the 6-311G(d,p) basis set would not exceed 0.01 eV in the bond dissociation energies, so we used the CP-uncorrected geometries throughout.

Results and Discussion

TOF Distributions and Breakdown Diagrams. TOF spectra were recorded in the photon energy range of 12.2−14.0 eV for chromocene, 12.8−14.4 eV for cobaltocene, and 11.7−13.2 eV for nickelocene. Typical time-of-flight distributions with the contribution of hot electrons subtracted are shown in Figure 1.

(34) Frisch, M. J., *Gaussian 03*, Revision E.01; Gaussian, Inc.: Wallingford, CT, 2004.
(35) (a) Becke, A. D. *J. Chem. Phys.* **1992**, *97*, 9173. (b) Becke, A. D. *J. Chem. Phys.* **1993**, *98*, 5648. (c) Lee, C.; Yang, W.; Parr, R. G. *Phys. Rev.* **1988**, *B37*, 785.
(36) (a) Krishnan, R.; Binkley, J. S.; Seeger, R.; Pople, J. A. *J. Chem. Phys.* **1980**, *72*, 650. (b) Blaudeau, J.-P.; McGrath, M. P.; Curtiss, L. A.; Radom, L. *J. Chem. Phys.* **1997**, *107*, 5016.
(37) Palm, H.; Alcaraz, C.; Millié, P.; Dutuit, O. *Int. J. Mass Spectrom.* **2006**, *249*, 31.
(38) Boys, S. F.; Bernardi, F. *Mol. Phys.* **1970**, *19*, 553.
(39) (a) Clark, T.; Chandrasekhar, J.; Spitznagel, G. W.; Schleyer, P. V. R. *J. Comput. Chem.* **1983**, *4*, 294. (b) Frisch, M. J.; Pople, J. A.; Binkley, J. S. *J. Chem. Phys.* **1984**, *80*, 3265. (c) Wachters, A. J. H. *J. Chem. Phys.* **1970**, *52*, 1033. (d) Hay, P. J. *J. Chem. Phys.* **1977**, *66*, 4377. (e) Krishnan, R.; Trucks, G. W. *J. Chem. Phys.* **1989**, *91*, 1062.

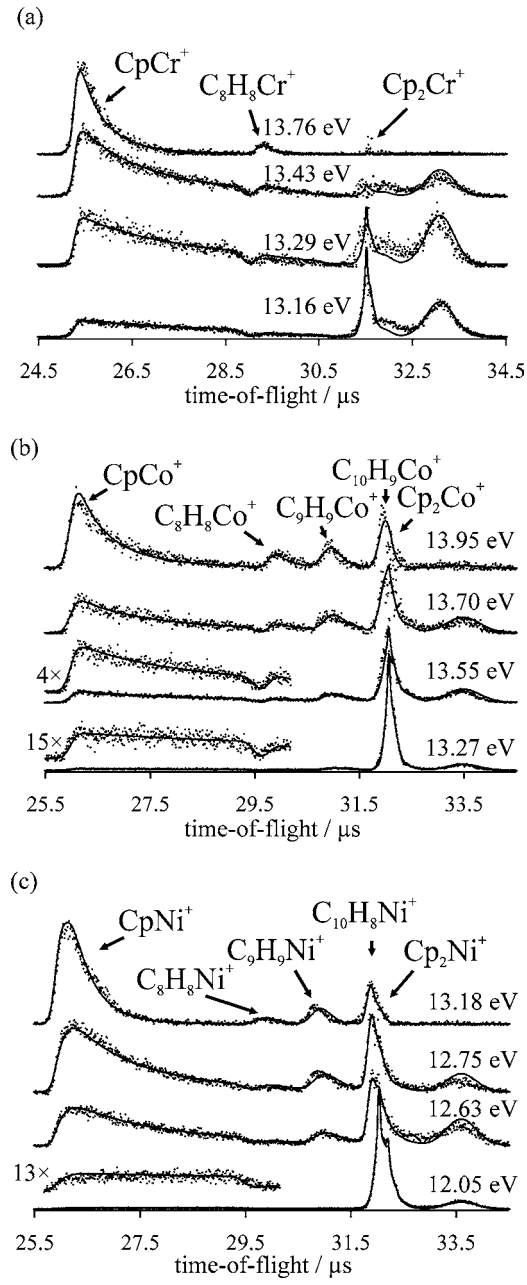

Figure 1. TOF distributions of (a) Cp_2Cr^+, (b) Cp_2Co^+, and (c) Cp_2Ni^+ at selected photon energies. Symbols are the experimental data, while the solid lines show the result of the SSACM simulation, as described under Data Analysis. Practically the same quality fit could be obtained with RAC-RRKM modeling.

The experimental data are represented by symbols, while the solid lines show the fitted TOF distributions, as discussed under Data Analysis. The major fragmentation belongs to cyclopentadienyl loss in all cases, but other minor channels appear as well. In the spectra of chromocene (Figure 1a) the peak at 31.5 μs belongs to the Cp_2Cr^+ molecular ion, whereas the fragment ions appear as asymmetric peaks between 25 and 29 μs and between 29 and 31 μs. The former is the $CpCr^+$, while the latter is due to C_2H_2 loss ($C_8H_8Cr^+$). The Cp_2Co^+ peak (Figure 1b) is at 32 μs. In a minor channel, the parent ion can lose a hydrogen atom, giving a peak at 31.9 μs, which cannot be separated from the parent ion peak in the linear time-of-flight experiment, but the TOF peak shape makes it clear that in this case it is an H-atom loss rather than an H_2-loss as for Cp_2Ni^+ (vide infra). The other fragment ions are $CpCo^+$ (25.5−29.5 μs), $C_8H_8Co^+$ (29.5−30.5 μs), and $C_9H_9Co^+$ (30.5−31.5 μs). In the TOF distributions of nickelocene (Figure 1c), the parent ion can be found at 32.0 and 32.2 μs (nickel has two major isotopes with an abundance ratio of about 5:2). The major fragmentation is Cp loss, giving $CpNi^+$ with a flight time between 25.6 and 29.6 μs. The peak at 31.9 μs, overlapping with the parent ion peak, is due to H_2 loss. The two most important dissociation channels in the nickelocene PEPICO TOF spectra are the direct loss of Cp ligand and the H_2 loss after isomerization of Cp_2Ni^+ to $C_{10}H_8NiH_2^+$. Two further fragments can also be seen in the TOF distributions, which belong to $C_8H_8Ni^+$ and $C_9H_9Ni^+$, at flight times of 29.7−30.6 μs and 30.6−31.6 μs, respectively. In all cases, the peaks on the right-hand side of the parent ions are the drift peaks (see below). As we mentioned earlier, the TOF distributions of nickelocene were also recorded with the reflectron setup, in order to investigate the H_2 loss with better mass resolution. It was found that only H_2 loss takes place and there is no H loss from the nickelocene ion. Because of the high bond energy of the H_2 molecule, it is very likely that instead of the sequential loss of two H atoms, the H_2 loss occurs in one step, and this dissociation channel follows the isomerization of Cp_2Ni^+ into a presumably $C_{10}H_8NiH_2^+$ ion. The maximum photon energy available in the instrument is about 14 eV, which is not sufficient to remove the cyclopentadienyl ligand from the CpM^+ ion (M = Cr, Co, Ni).

As is apparent from Figure 1, the molecular ion peaks comprise two parts: a central sharp peak on top of a broader peak. The sharp peak results from the effusive jet produced by the narrow sample inlet needle, while the broad feature is due to the metallocene vapor in the background. In the simulations (discussed later), we used two Gaussian functions with different full width at half-maximum values to convolute with the calculated intensity distributions of the parent ion. As shown in Figure 1, the daughter ion TOF distributions are asymmetric, and the so-called drift peaks can also be observed. This indicates slow dissociation: the ions dissociate while traveling in the first acceleration region or in the first drift region of the ion optics. If an ion dissociates in the acceleration region, its final velocity as it enters the drift region will be larger than that of the parent ion but less than that of a rapidly produced daughter ion. Thus, the total flight time of these slowly produced ions falls between that of the parent ion and that of the rapidly produced daughter ion. Because there is a distribution of lifetimes at a given dissociation rate, a quasi-exponential shape is observed in the product ion peak. The decay rate can be extracted from the analysis of the peak shapes. Similarly, if an ion dissociates in the first drift region, its final velocity as it leaves the deceleration region will be smaller than that of the parent, and as a result the total flight time of this ion will be larger than that of the parent ion. However, the drift peak due to the ions produced in the drift region is not asymmetric since all of these ions are decelerated to the same velocity before the second drift region.[22,40,41]

The TOF data in Figure 1 provide information about the absolute dissociation rates of the parent ions. If we plot the fractional abundance of the various ions as a function of the photon energy, we obtain the breakdown diagrams shown in Figure 2. These data provide information about the relative

(40) Kercher, J. P.; Gengeliczki, Z.; Sztáray, B.; Baer, T. *J. Phys. Chem. A* **2007**, *111*, 16.
(41) Hornung, B.; Bodi, A.; Pongor, C. I.; Gengeliczki, Z.; Baer, T.; Sztáray, B. *J. Phys. Chem. A* **2009**, *113*, 8091.

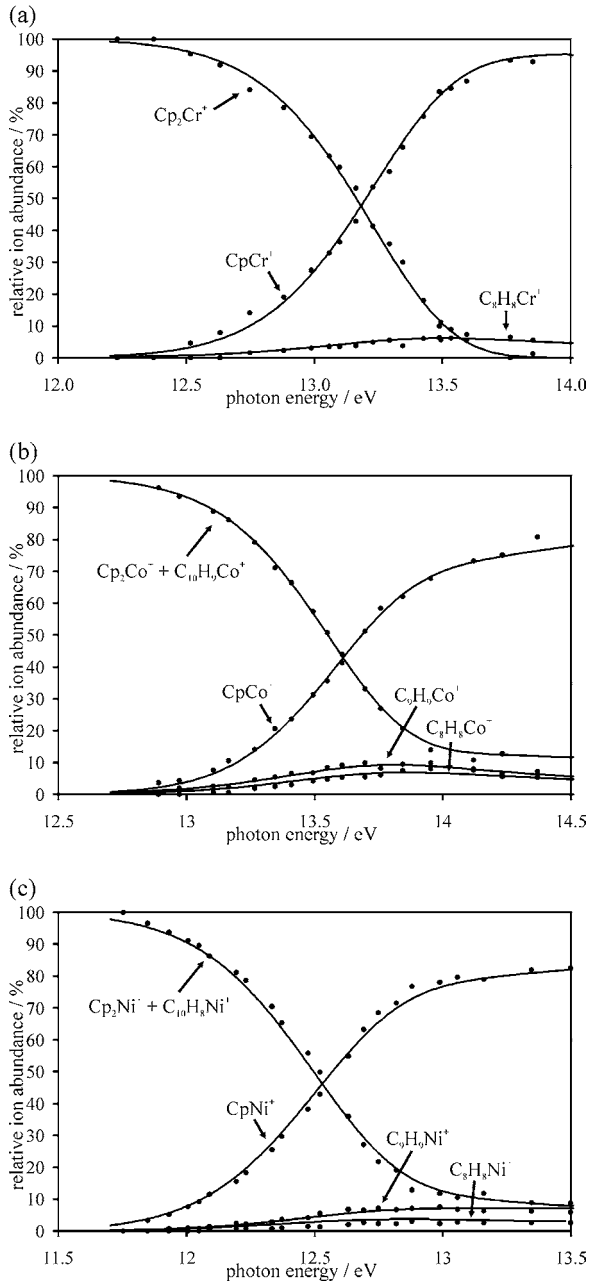

Figure 2. Breakdown diagrams of (a) Cp_2Cr^+, (b) Cp_2Co^+, and (c) Cp_2Ni^+. The symbols are the experimental data, while the solid lines show the SSACM calculated curves, as discussed in the text. The RAC-RRKM curves look essentially identical.

rates of ion formation. The symbols are the experimentally determined ratios after the hot electron subtraction; while the solid lines show the results of the simulations (see below).

Data Analysis. The thermal energy distribution of the neutral molecule and, therefore, the initial energy distribution of the molecular ions is much wider than the TPEPICO energy resolution (about 10 meV combined electron and photon resolution). Thus, the extraction of bond energies (E_0) from the experimental results requires an analysis of the dissociation rates in terms of the ion internal energy distributions. For energy selected (nonthermal) reactants, a commonly used model for calculating unimolecular rate constants is the RRKM theory[42,43] where the rate constant is given by the formula:

$$k(E) = \frac{\sigma N^{\ddagger}(E - E_0)}{h\rho(E)} \quad (1)$$

in which $N^{\ddagger}(E - E_0)$ is the sum of states of the transition state up to an internal energy of $E - E_0$ and $\rho(E)$ is the density of states of the dissociating ion measured from the bottom of the ion ground-state potential energy well. In the rigid activated complex (RAC) -RRKM model, the transitional modes are treated as vibrations with fixed frequencies. This is certainly appropriate for reactions with reverse barriers, in which the transition state is located at the critical point on the potential energy surface and does not change with internal energy. However, for reactions without a reverse barrier, the transition state (which is defined by an entropic minimum) shifts closer to the reactant along the reaction coordinate as the energy is raised. Variational transition-state theory (VTST) takes this explicitly into account. It was shown recently that even though the RAC-RRKM theory is capable of fitting the dissociation rates over a broad range (essentially from 10^3 to 10^9 s^{-1}), it can underestimate the bond dissociation energy by more than 0.1 eV when the kinetic shift is large.[44−46] In the TPEPICO study on halobenzene ions,[44] it was also shown that, contrary to RAC-RRKM, the simplified version of the statistical adiabatic channel model[45] (SSACM) not only fits the experimental rates properly but also was found to extrapolate to the known thresholds within the reported experimental errors. In addition, it requires similar computational effort as the RAC-RRKM method. The SSACM[45] is based on phase space theory (PST), which assumes that the decomposition of a molecule or collision complex is governed by the phase space available to each product under the conservation of energy and angular momentum, and the PST rate constant is thus calculated from the parameters of the products (rather than from an assumed fixed transition state). The SSACM rate constant takes the anisotropy of the potential energy surface into account by multiplying the transitional rotational number of states by an energy-dependent rigidity factor. For the loss of a polarizable neutral fragment with no dipole moment (such as Cp), a useful form of the factor is given by

$$f_{\text{rigid}}(E) = \exp\left[-\frac{E - E_0}{c}\right] \quad (2)$$

where c is an adjustable parameter that indicates the relative contribution of the isotropic long-range part of the potential in comparison to the anisotropic short-range part.

The large number of internal degrees of freedom in neutral metallocene molecules and the asymmetric peak shape of the CpM^+ ions in the TOF distributions over a wide energy range indicate a very significant kinetic shift for the Cp loss from Cp_2M^+. Therefore, in the modeling of the TPEPICO data, both RAC-RRKM and SSACM were employed, the latter rate theory to obtain accurate and reliable thermochemistry of these ions

(42) Baer, T.; Hase, W. L. *Unimolecular Reaction Dynamics: Theory and Experiments*; Oxford University Press: New York, 1996.
(43) (a) Kassel, L. S. *J. Phys. Chem.* **1928**, *32*, 225. (b) Marcus, R. A.; Rice, O. K. *J. Phys. Colloid Chem.* **1951**, *55*, 894. (c) Rice, O. K.; Ramsperger, H. C. *J. Am. Chem. Soc.* **1927**, *49*, 1617.
(44) Stevens, W.; Sztáray, B.; Shuman, N.; Baer, T.; Troe, J. *J. Phys. Chem. A* **2009**, *113*, 573.
(45) Troe, J.; Ushakov, V. G.; Viggiano, A. A. *J. Phys. Chem. A* **2006**, *110*, 1491.
(46) Shuman, N. S.; Bodi, A.; Baer, T. *J. Phys. Chem. A* **2010**, *114*, 232.

and RAC-RRKM as a comparison to both literature data and to obtain the model uncertainty of the final values.

The adiabatic ionization energies of Cp_2M (M = Cr, Co, Ni) are also necessary for the data analysis. There are several vertical ionization energy values of metallocenes in the literature, derived from HeI photoelectron spectra. Rabalais[47] determined the IE of Cp_2M to be 5.69 and 6.40 eV (no error bars given) for M = Cr and Ni, while values of 5.70 ± 0.1 eV (Cp_2Cr), 5.55 ± 0.1 eV (Cp_2Co), and 6.50 ± 0.1 eV (Cp_2Ni) were published by Cauletti et al.[48] These latter values are in good agreement with Evans et al.,[49] who suggested vertical ionization energies of 5.71, 5.56, and 6.51 eV (no error bars given) for Cp_2M where M = Cr, Co, and Ni, respectively. While the vertical IE is readily determined from the peak maximum in the photoelectron spectrum, the adiabatic IE is more difficult to extract from a broad band and, accordingly, the adiabatic values of 5.50 eV (Cp_2Cr) and 6.20 eV (Cp_2Ni) by Rabalais,[47] listed without confidence intervals, are of uncertain accuracy. Thus, the adiabatic ionization energies used in the modeling were calculated instead from the experimental Gibbs free energies of ionization of 533.5 kJ/mol (5.529 ± 0.065 eV) for Cp_2Cr, 516.7 kJ/mol (5.355 ± 0.065 eV)[50] for Cp_2Co, and 601.7 kJ/mol (6.236 ± 0.065 eV)[51] for Cp_2Ni. These values, published by Ryan et al.,[50,51] were determined by Fourier transform ion cyclotron resonance mass spectrometry in which gas-phase electron-transfer equilibrium reactions were investigated between the metallocenes and a variety of reference compounds whose adiabatic ionization energies are well-known. In order to convert these ΔG_{ioniz} values to ΔH_{ioniz}, we used the calculated ΔS_{ioniz} of −1.10, −43.03, and −3.82 $J \cdot mol^{-1} \cdot K^{-1}$ for Cp_2Cr, Cp_2Co, and Cp_2Ni, respectively. The entropic contribution of the Cp-ring rotation−essentially a free rotor in all cases−was assumed to cancel out for the Cp_2M and Cp_2M^+ complexes[51,52] and was thus neglected in calculating ΔS_{ioniz}. The multiplicities and orbital degeneracies were used to calculate the electronic entropies, assuming ground-state to ground-state transitions. The entropy of ionization of cobaltocene is quite different from the other two metallocenes because the cobaltocene assumes the very stable 18-electron configuration upon the ejection of an antibonding electron, which results in a significant entropy decrease, largely due to the tightening of the vibrational modes. The ionization entropies yield $T\Delta S$ terms of −0.004, −0.156, and −0.014 eV for Cp_2M where M = Cr, Co, and Ni, respectively, at 350 K (the temperature of the electron-transfer experiment). From these values, we obtained ΔH_{ioniz}(350 K) of 5.52 eV (Cp_2Cr), 5.20 eV (Cp_2Co), and 6.22 eV (Cp_2Ni). These can be converted to ΔH_{ioniz}(0 K), the adiabatic IE, by use of calculated $H_{350K} - H_{0K}$ values, which finally yields the adiabatic ionization energies of 5.53, 5.24, and 6.22 eV for our three compounds. The error in the electron transfer equilibria were quoted as ±6 kJ/mol,[50,51] while the conversion to ΔH_{ioniz}(0 K) is likely to contribute an error less than 2 kJ/mol (0.02 eV) for the chromium and nickel complexes and 5 kJ/mol (0.05 eV) for the cobalt complex, which undergoes significant tightening upon ionization. Therefore, the adiabatic ionization energies that we used in our data analysis are 5.53 ± 0.07 eV (Cp_2Cr), 5.24 ± 0.08 eV (Cp_2Co), and 6.22 ± 0.07 eV (Cp_2Ni). These numbers, coming from equilibrium measurements, are currently the most reliable available ionization energies and are in very good agreement with the Rabalais adiabatic IEs determined from photoelectron spectra.

The RAC-RRKM fit of the TOF distributions and breakdown diagram can be calculated from the following information: the adiabatic ionization energy; the thermal energy distribution of neutral Cp_2M (M = Cr, Co, Ni) molecules, leading to the internal energy distribution of the dissociating ions; the ion optics parameters (acceleration electric fields and the acceleration and drift distances); and the transition-state vibrational frequencies. We use the density of rovibrational states calculated by the direct count method[53] to determine the thermal energy distribution of the neutral molecule. The harmonic frequencies and rotational constants were determined by quantum chemical calculations as discussed above. Since our DFT calculations indicate that the energy barrier of the Cp ring rotation is less than 5 kJ/mol for each metallocene, the lowest frequency mode of metallocenes, which is assigned as the internal rotation of the Cp ring, was treated as a hindered (Pitzer) rotor.[42,54] The necessary moments of inertia were obtained from the calculated structure of the equilibrium states, while for the barrier heights, the DFT estimated values were used. The energy distribution of the molecular ion is obtained as the convolution of the combined electron and photon energy resolution function with the energy distribution of the neutral molecule. The microcanonical dissociation rates were calculated by use of eq 1. The dissociation limits and the lowest five TS vibrational frequencies were adjusted together until the best fit was obtained to both dissociation rates (from the TOF distributions) and breakdown curves. These frequencies were significantly lower than the initial estimate from the constrained DFT optimization at a fixed metal-to-Cp distance, indicating a loose transition state. The averages of the varied lowest five frequencies were 33, 7, and 14 cm^{-1} for $[CpM^+ \cdots Cp]$ where M = Cr, Co, and Ni, respectively. The fact that RAC-RRKM models the transitional modes as very low-frequency vibrations is clearly not a very good approximation (vide infra). The forward and backward barriers of the isomerization process of nickelocene ion and the lowest few frequencies of the isomerization transition state were obtained from analysis of the reflectron measurements and were used without fitting in the modeling of the linear TOF experiments. The following 0 K appearance energies were determined for the CpM^+ fragment ions: 10.14 ± 0.10, 10.83 ± 0.11, and 9.88 ± 0.14 eV for M = Cr, Co, and Ni, respectively.

The uncertainties for the appearance energies were estimated by testing the sensitivity of the fit to the assumed vibrational frequencies. The lowest five transition-state frequencies were multiplied and divided by various factors and the fitting procedure of the appearance energies was carried out with these fixed values. This scheme simulates looser and tighter transition states, thereby altering the $k(E)$ curves. Increasing the amount of this alteration changes the fitted E_0 value and deteriorates the fit; the error bar for the E_0 can be determined from the points where the fit becomes unacceptable. It was found that, upon changing the frequencies by ±30%, the quality of the fit to the

(47) Rabalais, J. W. *J. Chem. Phys.* **1972**, *57*, 1185.
(48) Cauletti, C.; Green, J. C.; Kelly, M. R. *J. Electron Spectrosc. Relat. Phenom.* **1980**, *19*, 327.
(49) Evans, S.; Green, M. L. H.; Jewitt, B.; King, G. H.; Orchard, A. F. *J. Chem. Soc., Faraday Trans. 2* **1974**, *70*, 356.
(50) Ryan, M. F.; Richardson, D. E.; Lichtenberger, D. L.; Gruhn, N. E. *Organometallics* **1994**, *13*, 1190.
(51) Ryan, M. F.; Eyler, J. R.; Richardson, D. E. *J. Am. Chem. Soc.* **1992**, *114*, 8611.
(52) Richardson, D. E.; Sharpe, P. *Inorg. Chem.* **1993**, *32*, 1809.
(53) Beyer, T.; Swinehart, D. R. *Commun. ACM* **1973**, *16*, 379.
(54) Pitzer, K. S. *Quantum Chemistry*; Prentice-Hall: New York, 1953.

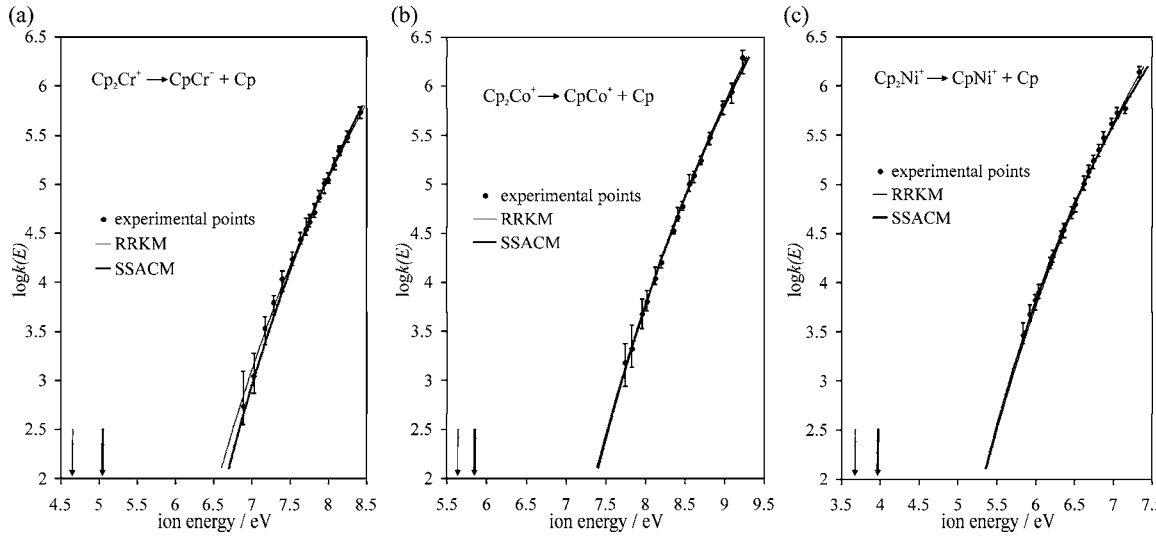

Figure 3. Comparison of rate curves predicted by RAC-RRKM and SSACM models fit to experimentally determined rate points of cyclopentadienyl loss from (a) Cp_2Cr^+, (b) Cp_2Co^+, and (c) Cp_2Ni^+. Dotted arrows show the extrapolated dissociation thresholds. Determination of the error bars in rate points is described in the text.

TOF distributions became significantly worse, and the obtained E_0 values were then accepted as the error bars. It is worth noting that this alteration did not affect the simulated breakdown diagram significantly. This is indeed the expected behavior, as the quasi-exponential shape of the asymmetric daughter ion TOF distributions depends on the absolute dissociation rate, whereas the breakdown diagram depends only on the ratio of the rate constants and is, therefore, unable to estimate the kinetic shift.

The SSACM modeling was done analogously. Dissociation rates were calculated by multiplying the transitional rotational number of states by the energy-dependent rigidity factor given in eq 2. The frequencies of product ions and neutrals were obtained from quantum chemical calculations as discussed above. Since SSACM is limited to reactions with no reverse activation energy, the isomerization process of nickelocene was treated with the RAC-RRKM theory. In these modeling calculations, the dissociation limits and the SSACM *c* parameters were optimized to fit the time-of-flight distributions and breakdown curves to the experimental data. The role of these optimized energy-dependent rigidity factors is to correct the PST rates to the experimentally measured values, and the optimized values were 279, 1942, and 581 cm^{-1} for Cp_2Cr^+, Cp_2Co^+, and Cp_2Ni^+, respectively. Without this SSACM correction, in the range of the experimental rate constants, the PST rates were 1.1−1.4 orders of magnitude faster than the SSACM rates for the nickelocene ions. While the difference for cobaltocene was somewhat smaller, for chromocene the fastest measured rate was more than 2 orders of magnitude slower than the PST calculated one, if the same E_0 is assumed. The best fit to the TOF distributions and breakdown diagrams was obtained with the 0 K appearance energies for $CpCr^+$, $CpCo^+$, and $CpNi^+$ of 10.57 ± 0.10, 11.01 ± 0.08, and 10.18 ± 0.09 eV, respectively. The error bars of the appearance energies were obtained by repeating the fitting procedure with various fixed *c* parameters. The simulated time-of-flight distributions and breakdown diagrams are shown as solid curves in Figures 1 and 2. Although the results of the SSACM analysis are shown in the figures, we could get practically the same quality of fit with RAC-RRKM modeling, as well.

The agreement between the calculated and measured breakdown curves and TOF distributions is very good; even the branching ratios of the C_2H_2-loss channel from Cp_2Cr^+ could be reproduced with suitable accuracy by modeling this channel as a direct dissociation, although isomerization might play a role here. We have checked the importance of the CH and C_2H_2 losses in the modeling of the two other metallocenes. It turned out that neglect of the minor channels decreases the determined CpM^+ appearance energies by approximately 30 meV. The RAC-RRKM appearance energies are systematically smaller than the SSACM values, by up to 0.4 eV in the case of $CpCr-Cp^+$. The considerably larger difference between RRKM and SSACM in the case of the $[CpCr-Cp]^+$ reaction compared to the halobenzene dissociation[44] is the much slower reaction in the former and thus the much larger kinetic shift. As evident in the breakdown diagram for $CpCr-Cp^+$ in Figure 2a, the derived dissociation onset of 10.57 eV is about 2 eV below the phenomenological onset, which greatly increases the extrapolation error in the RRKM model.[44] The RAC-RRKM and SSACM calculated rate curves for the cyclopentadienyl-loss channels are shown in Figure 3 along with the experimentally determined rate points. The experimental rate constants were determined at each photon energy by fitting the TOF distribution with a $k(E)$ function weighted by the thermal energy distribution. The fitting was carried out only over the thermal energy distribution. At each photon energy, we obtained one $k(E)$ value, where $E = h\nu - \mathrm{IE} + E_{th}$ and E_{th} is the most probable energy in the thermal energy distribution. The error limits were established by varying the $k(E)$ function until the fit to the TOF distribution at the given photon energy no longer seemed reasonable. It is evident that both the RAC-RRKM and the SSACM models fit the rates over 3 orders of magnitude in the experimental $k(E)$ values. A remarkable feature of the $k(E)$ curves in Figure 3 is the 2 eV extrapolation (kinetic shift) of the rate curves from the lowest measured value to the onset and the very small rate constant at the dissociation limit. Even 3 eV above the 0 K onsets, the dissociation is still metastable. The activation entropy is more than 50 $J \cdot K^{-1} \cdot mol^{-1}$ at 600 K for all of the investigated metallocene ions; these large positive values indicate that the dissociation of Cp proceeds via a loose transition state, as expected for simple bond-breaking reactions.

Although we cannot distinguish the two rate models by the goodness of the fit, we note that the RRKM theory, which

Table 1. Experimental, Calculated, and Literature $[CpM-Cp]^+$ Bond Dissociation Energies and Molecular Orbital Occupation of Metallocene Ions

	bond dissociation energies (eV)				orbital occupation[a]	
	TPEPICO[c]					
	RAC-RRKM	SSACM	calcd[b]	selected literature	CpM^+	Cp_2M^+
Cp_2Cr^+	4.61 ± 0.12[d]	5.04 ± 0.12[d]	4.0	6.55 ± 0.15[e]	$e_2^2\, a_1^1\, e_1^1$	$e_{2g}^2\, a_{1g}^1$
Cp_2Mn^+	3.43 ± 0.17[f]		2.8		$e_2^2\, a_1^1\, e_1^2$	$e_{2g}^2\, a_{1g}^1\, e_{1g}^1$
Cp_2Fe^+			2.9	3.7 ± 0.3,[g] 3.95 ± 0.5,[h] 6.7 ± 0.2[i]	$e_2^3\, a_1^1\, e_1^2$	$e_{2g}^3\, a_{1g}^2$
Cp_2Co^+	5.59 ± 0.14[d]	5.77 ± 0.11[d]	4.8	7.79 ± 0.15,[e] 6.3 ± 1.0,[j] 4.86 ± 0.5[k]	$e_2^4\, a_1^1\, e_1^2$	$e_{2g}^4\, a_{1g}^2$
Cp_2Ni^+	3.66 ± 0.16[d]	3.96 ± 0.11[d]	3.0	5.43 ± 0.15,[e] 5.16 ± 0.1,[j] 3.24 ± 0.07[l]	$e_2^4\, a_1^2\, e_1^2$	$e_{2g}^4\, a_{1g}^2\, e_{1g}^1$

[a] Cauletti et al.[48] and Evans et al. [49] [b] B3LYP/6-311G++(2df,2pd)//B3LYP/6-311G(d,p). [c] Recommended values with the model uncertainty taken into account: 5.04 ± 0.16 eV for Cp_2Cr, 5.77 ± 0.15 eV for Cp_2Co, and 3.96 ± 0.15 eV for Cp_2Ni. [d] This study. [e] Müller and D'Or.[23] [f] Li et al. [17] [g] Faulk and Dunbar.[59] [h] Han et al.[60] [i] Barfuss et al.[61] [j] Pignataro and Lossing.[25] [k] Opitz.[28] [l] Lin and Dunbar.[31]

assumes a fixed transition state, is not accurate for barrierless dissociation reactions with a very large kinetic shift. The SSACM model, although not rigorous, has the virtue that it extrapolates to the correct model (phase space theory) for such reactions. In the only quantitative test of SSACM, the halide loss from the halobenzene ions, the derived SSACM onsets were correct to within the experimental uncertainty of the known thermochemistry (±20 meV). Furthermore, it was noted in that study that the accuracy of the fit is greatly improved by good rate data down to $10^3\ s^{-1}$, which is close to the lowest rate that can be measured without interference from IR radiative cooling.[55] Even when it is considered that the kinetic shift is much larger here than in the case of the halobenzenes, the uncertainty from the SSACM modeling is no more than 0.1 eV. When this uncertainty is added into the SSACM error derived from the fitting quality, we arrive at the following recommended 0 K appearance energies: 10.57 ± 0.14 eV for Cp_2Cr, 11.01 ± 0.13 eV for Cp_2Co, and 10.18 ± 0.13 eV for Cp_2Ni.

From the CpM^+ E_0 values (M = Cr, Co, Ni) and adiabatic ionization energies, we obtained the $[CpM-Cp]^+$ bond dissociation energies via $D_0 = E_0[CpM^+] - IE[Cp_2M]$. This yields 0 K ionic bond dissociation energies of 5.04 ± 0.16, 5.77 ± 0.15, and 3.96 ± 0.15 eV for M = Cr, Co, and Ni, respectively. The derived and literature bond energies with the obtained uncertainties are summarized in Table 1. As usual, the early electron impact appearance energies and bond dissociation energies are much larger than the TPEPICO values.[23,25−27,29,30] Interestingly, the most recent electron ionization study of Opitz[28] suggests a $CpCo^+$ appearance energy of 10.21 eV and $[CpCo-Cp]^+$ bond energy of 4.86 ± 0.5 eV, which is significantly lower than our result, possibly due to neglect of the thermal energy distribution in data analysis. A time-resolved photodissociation study using an RRKM model gave a $[CpNi-Cp]^+$ bond energy of 3.24 ± 0.07 eV,[31] smaller than our SSACM values by about 0.7 eV. The large difference can be attributed to the lack of detailed rate data as the calculated RRKM rate curve was fitted to only two rate points. It is important to note, however, that the lower rate point in this experiment is clearly far outside the uncertainty of either the SSACM or the RAC-RRKM rate curves that fit to our measured dissociation rates, possibly due to comparable IR emission rate at this energy. Also, the use of RAC-RRKM is likely to contribute a difference of several tenths of electronvolts compared to SSACM.[44−46]

Our experimentally determined bond dissociation energies (BDEs) were compared to calculations at the B3LYP/6-311++G(2df,2pd)// B3LYP/6-311G(d,p) level of theory. It seems that the agreement between calculated and measured values is only moderate; the B3LYP results are systematically 0.9−1.0 eV lower than the SSACM and 0.6−0.8 eV lower than the RRKM BDE values. However, the BDE trends between the three compounds studied in this work and manganocene from a previous TPEPICO study are reproduced even at this level of theory.

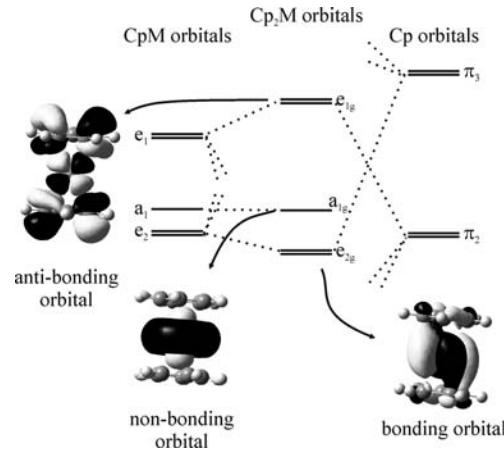

Figure 4. Part of the molecular orbital structure of metallocenes and its formation from CpM and Cp fragments.

Bond Dissociation Energy Trend. The trends in the $[CpM-Cp]^+$ BDEs along the first row of transition metals can be interpreted qualitatively on the basis of electronic structure changes upon dissociation. In Figure 4, we depict the orbital interactions upon the formation of Cp_2M from CpM and Cp fragments. For the metallocenes, only the orbitals with varying occupation numbers are indicated; a detailed description of the orbital structures of Cp_2M and CpM can be found in the organometallic literature.[56] The labeling in Figure 4 corresponds to D_{5d} and C_{5v} symmetries. The e_{2g} orbital of Cp_2M has a bonding character with respect to the CpM−Cp bond, due to the favorable overlap of π_3 and the metal-centered lobes of e_2, while e_{1g} is an antibonding combination originating mainly from e_1 and π_2. [Note that the increase of symmetry puts restrictions on how the fragment orbitals will mix to form these higher-symmetry orbitals (see ref 56), but this does not affect the present considerations.] Both a_1 and a_{1g} are essentially nonbonding metal-centered d_{z^2}-type orbitals with 4−8% s character.

Interpretation of BDE changes along the Cr ... Ni series is now possible if we examine the stepwise changes in the

(55) (a) Asamoto, B.; Dunbar, R. C. *J. Phys. Chem.* **1987**, *91*, 2804. (b) Dunbar, R. C.; Chen, J. H.; So, H. Y.; Asamoto, B. *J. Chem. Phys.* **1987**, *86*, 2081.

(56) Albright, T. A. *Tetrahedron* **1982**, *38*, 1339.

electronic configuration of CpM^+ and Cp_2M^+. It must be noted that the following analysis neglects the correlation interaction among the electrons, the variation of metallocene orbital energies with the metal, and the Jahn−Teller distortion; it is therefore not expected to explain all subtleties of the BDE trends. On the basis of the low coordination number and analogous literature results for benzene complexes,[57] we assume that all CpM^+ species to have high-spin configurations involving the e_2, a_1, and e_1 orbitals. Our DFT calculations indeed confirm this assumption. [For $CpCo^+$, the low-spin $e_2^4\ a_1^2\ e_1^1$ configuration was found to have practically the same energy as the high-spin state configuration.] These orbital occupations (from $e_2^2\ a_1^1\ e_1^1$ for Cr up to $e_2^4\ a_1^2\ e_1^2$ for Ni) of the CpM^+ ions are listed in Table 1. For the Cp_2M^+ ions, the electronic configurations were obtained from HeI photoelectron spectra,[48,49] and these configurations, along with the bond dissociation energy values, are summarized in Table 1. As found by Long,[58] simple quantum-chemical calculations could not always reproduce the most stable configurations; in this analysis we used the experimental ones.

The bond energy data of the manganocene ion comes from an earlier TPEPICO study[17] while for the $[CpFe-Cp]^+$ dissociation energy, there is no agreement in the literature on a reliable bond energy. Table 1 lists two low values, both based on time-resolved laser photodissociation experiment by Faulk and Dunbar.[59] The slightly higher value of 3.95 eV[60] uses one extra rate point to correct the RRKM extrapolation in the original Dunbar paper. A photoionization mass spectrometry study by Barfuss et al.[61] concludes a $[CpFe-Cp]^+$ bond energy that is 3 eV higher but fails to take kinetic shift into account and, therefore, represents only a far upper limit.

In order to understand the trends in the bond energies, one has to consider the trend in the changes upon dissociation (or, oppositely, upon bond formation) rather than just the trend in the Cp_2M^+ molecular orbital occupations themselves. The clearest argument for this is probably the striking difference between the Cr−Mn and Co−Ni pairs, where the addition of an extra e_{1g} electron results in a BDE decrease of 1.2 eV versus 1.8 eV. For all five metallocenes considered, after bond formation the electrons originally occupying the a_1 and e_2 orbitals in CpM^+ are now on the a_{1g} and e_{2g} orbitals, respectively. Also, a common motif is that one e_1 electron together with the three Cp π_2 electrons completes the doubly degenerate bonding orbital formed by the overlap of the e_1 and the π_2 orbitals. The main difference in the series is what happens to the other e_1 electron. For Mn and Ni, the extra electron is promoted to the antibonding e_{1g} orbital, while for Fe and Co, it is stabilized on the a_{1g} orbital. In $CpCr^+$, there is no second e_1 electron. According to this, Cp_2Fe^+ and Cp_2Co^+ should have the highest BDE and Cp_2Mn^+ and Cp_2Ni^+ should have the least stable bond, with Cp_2Cr^+ in between. The difference between bonding in the manganocene and nickelocene ions is the stabilization of two extra e_2 electrons to the e_{2g} orbital due to favorable overlap with the π_3 orbital of the Cp ring. Therefore, Cp_2Ni^+ is likely to have a higher BDE than Cp_2Mn^+. Similar arguments hold between the ferrocene and cobaltocene ions, with the latter having an extra e_2 electron. Furthermore, the cobaltocene ion exhibits the most stable 18-electron configuration, which results in extra stabilization. This is in line with the calculations on the entropy of ionization, as well. The above arguments suggest a BDE trend of $Cp_2Mn^+ < Cp_2Ni^+ < Cp_2Cr^+ < Cp_2Fe^+ < Cp_2Co^+$. Comparison with the experimental BDE values in Table 1 indeed confirms this trend with the notable exception of ferrocene, for which we do not have TPEPICO data, due to the high ionization energy. If the above considerations based on orbital occupation are correct, the bond energy from the laser photodissociation study of Faulk and Dunbar[59] is probably too low, and a synchrotron-based PEPICO study of ferrocene is warranted.

Conclusions

Threshold photoelectron photoion coincidence spectroscopy was used to investigate the dissociation kinetics of the Cp_2M^+ (M = Cr, Co, Ni) ions. The dissociation of the Cp_2M^+ ions proceeds by the parallel loss of neutral cyclopentadienyl ligand, CH, and C_2H_2 groups. Cobaltocene ion also loses an H atom. In addition, DFT calculations indicate that isomerization of nickelocene occurs, yielding a complex with pentafulvalene ($C_{10}H_8$) and H_2 ligands. By fitting the metastable ion time-of-flight distributions and the breakdown diagrams with the statistical SSACM model, reliable 0 K appearance energies were obtained for the fragment ions CpM^+ (M = Cr, Co, Ni). In accordance with an earlier study,[44] a comparison of the rigid activation complex RRKM model with SSACM indicates that both theories are capable of fitting the rates over a broad range, but RAC-RRKM predicts significantly lower bond energies. The adiabatic ionization energy of the metallocenes, calculated from the reported Gibbs free energies, leads to the metal−Cp bond dissociation energies in Cp_2M^+. The trend in the experimental M−Cp bond dissociation energies determined in this work agrees well with a simple molecular orbital picture of the electronic structure of the Cp_2M^+ and CpM^+ ions with the notable exception of Cp_2Fe^+, for which there is no PEPICO data available.

Acknowledgment. We are grateful to the U.S. Department of Energy for financial support as well as to the International Office of the U.S. National Science Foundation and the Hungarian National Science Fund (Grants OTKA NN71044 and F60679) for supporting this work. B.Sz. gratefully acknowledges the financial support of the ACS Petroleum Research Fund. Á.R. acknowledges a grant from Richter Gedeon Centenary Foundation (RGCA).

Supporting Information Available: Full citation for ref 34. This information is available free of charge via the Internet at http://pubs.acs.org.

JA105511T

(57) Meyer, F.; Khan, F. A.; Armentrout, P. B. *J. Am. Chem. Soc.* **1995**, *117*, 9740.
(58) Long, N. J. *Metallocenes: An Introduction to Sandwich Complexes*, 1st ed.; Wiley−Blackwell: London, 1998.
(59) Faulk, J. D.; Dunbar, R. C. *J. Am. Chem. Soc.* **1992**, *114*, 8596.
(60) Han, S.-J.; Yang, M. C.; Hwang, C. H.; Woo, D. H.; Hahn, J. R.; Kang, H.; Chung, Y. *Int. J. Mass Spectrom.* **1998**, *181*, 59.
(61) Barfuss, S.; Emrich, R.-H.; Hirschwald, W.; Dowben, P. A.; Boag, N. M. *J. Organomet. Chem.* **1990**, *391*, 209.